ACS APPLIED ELECTRONIC MATERIALS

Article

Cite This: ACS Appl. Electron. Mater. 2020, 2, 134−139

pubs.acs.org/acsaelm

Photovoltaic and Photoconductive Action Due to PbS Quantum Dots on Graphene/SiC Schottky Diodes from NIR to UV

Mathew L. Kelley,[†] Joshua Letton,[‡] Grigory Simin,[‡] Fiaz Ahmed,[†] Cole A. Love-Baker,[§] Andrew B. Greytak,*[,†,∥] and M. V. S. Chandrashekhar*[,‡]

[†]Department of Chemistry and Biochemistry, [‡]Department of Electrical and Computer Engineering, [§]Department of Chemical Engineering, and [∥]USC Nanocenter, University of South Carolina, Columbia, South Carolina 29208, United States

Supporting Information

ABSTRACT: We demonstrate photovoltaic and photoconductive responses to near-infrared light in devices formed by depositing a film of gel permeation chromatography purified PbS quantum dots (QDs) on top of n-SiC epitaxial layers with natively grown, low-leakage 10−15 monolayer thick epitaxial graphene (EG) Schottky contacts. The QD film layer was removable by selective chemical etching, resetting the EG/SiC Schottky diode: the sub-bandgap response could be restored in subsequent PbS-QD depositions. The EG in these devices simultaneously forms Schottky contacts to SiC and ohmic contacts to PbS-QD, enabling electrical screening and isolation of these interfaces from each other. After PbS-QD deposition, the diodes exhibit photovoltaic and photoconductive responses at photon energies far below the SiC bandgap, extending to the NIR gap of the QD film. Scanning photocurrent microscopy illustrates that this is due to charge transfer from the QD film to the n-type 4H-SiC through a trap-limited, rectifying PbS-QD/SiC heterojunction with ideality $n = 2$ in parallel with the EG/SiC Schottky diode. The photoconductive gain at this QD/SiC interface could be useful for IR detection in wide-bandgap platforms. Response times as fast as 40 ms are suitable for imaging applications, although careful contact design is required to optimize work-function matching and spreading resistance.

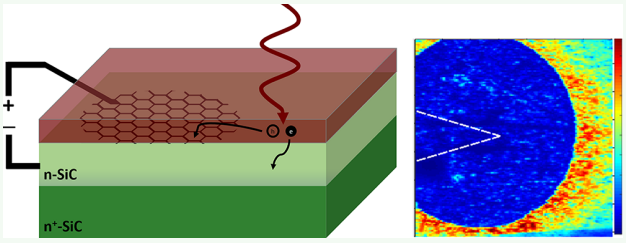

KEYWORDS: *quantum dot, lead sulfide, silicon carbide, GPC, photovoltaic, scanning photocurrent microscopy*

INTRODUCTION

Colloidal semiconductor QDs such as PbS[1,2] notably demonstrate size-tunable luminescence and optical absorption with effective bandgaps spanning from violet to mid-infrared. These characteristics together with solution processability have sparked interest in QDs as the absorber in thin film and hybrid devices such as solar cells and infrared focal plane array detectors.[3] The most successful QD solar cell designs currently rely on photoinduced electron transfer across a heterojunction with a reducible (n-type) wide-bandgap (WBG) metal oxide (e.g., TiO_2 or ZnO) as a key driver of charge separation. The demonstration of >10% efficiency in QD solar cells has shown the promise of this approach,[3,4] but open circuit voltages and short circuit currents remain below theoretical limits. It is thus important to consider junctions between QD films and other WBG semiconductors favorable for charge separation and strategies for making ohmic contacts for high carrier extraction. However, small variations in dimensional control and surface termination during the synthesis of QDs and formation of QD solids can have large effects on performance.[5,6]

The goal of this work is to investigate charge separation due to light at a wide-bandgap SiC/PbS QD film interface. The introduction of narrow-gap materials such as PbS onto WBG materials is compelling as it introduces the potential for engineered near-infrared (NIR) optoelectronic functionality in WBG devices. By using spin-coated QD-films, we eliminate the need for the constraints of epitaxial registry in more traditional thin film crystal growth. Other nonepitaxial deposition techniques such as chemical vapor deposition and sputtering also suffer from high cost and restrictions with material compatibility due to thermal budget and contamination issues.[7]

One challenge with electrical characterization of WBG/QD structures such as PbS-QD/SiC is the difficulty in forming reproducible contacts to composite materials such as the QD-film. Depending on the morphology of the PbS-QD film on SiC, contacts such as evaporated top metals have the potential to short through the QD films and create uncertainties in interpretation of optoelectronic data. Other challenges stem from uncertainties in the work function of the PbS-QD film. Depending on the ambient condition, the effective polarity of QD films with the same nominal surface termination can vary from n-type in vacuum photoelectron spectroscopy[8,9] to p-type after exposure to humid air.[10,11] There may also be carrier trapping at rectifying regions in the metal/QD film interface, leading to poor ideality.[12] These major issues present a serious challenge in the choice of metallization for characterization of QD/WBG heterojunctions.

Received: October 4, 2019
Accepted: December 10, 2019
Published: December 10, 2019

DOI: 10.1021/acsaelm.9b00651
ACS Appl. Electron. Mater. 2020, 2, 134−139

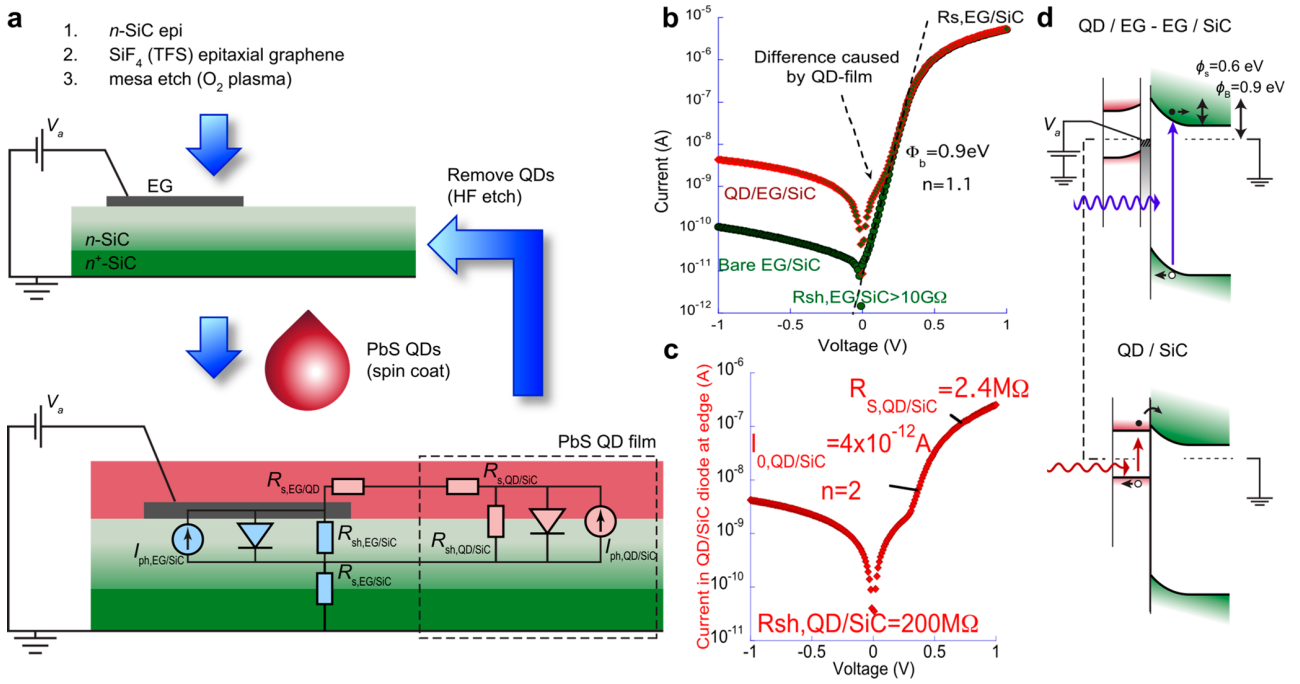

Figure 1. (a) Device assembly and architecture indicating continuous QD film and n-SiC epilayer with patterned EG mesa. Superimposed is an equivalent circuit representation of the EG/SiC and QD/SiC interfaces indicating the spreading resistance of the QD film and shunt resistance contributed by the QD/SiC interface (dashed box). (b) Dark DC $I-V$ characteristics for the bare and QD-coated devices. (c) Isolated QD/SiC junction $I-V$ behavior. (d) Energy band diagrams of the constituent diodes shown in (a) illustrating ohmic contact between QDs and EG.

We have recently explored optoelectronic properties of Schottky diodes and bipolar phototransistors based on the tetrafluorosilane (SiF_4, TFS) grown contacts of epitaxial graphene (EG) on a SiC substrate to form a graphene/WBG interface.[13−15] These devices are sensitive to ultraviolet light based on the bandgap of 4H-SiC. Here, we demonstrate that these devices respond to NIR light as a direct consequence of the rectifying junction formed between the QD film and n-type 4H-SiC. The QD-graphene interface has been examined in other recent studies wherein charge transfer FETs built with QDs and exfoliated or deposited graphene[6,10] demonstrated an optical responsivity up to 10^8 A/W. The QD-graphene interface was also examined in similar devices utilizing single-layer epitaxial graphene (EG),[16−18] and additionally in barristor-type devices in which the graphene−Si Schottky barrier height is modulated by charge transfer from QDs.[19,20] In many of these studies the varying carrier density in the graphene is the key mode of operation. However, the lone remaining junction of QD/WBG-SiC has not been isolated, partly due to the complexity of the interplay between the various junctions.

In this paper, we create spatially and electronically separated QD/EG and QD/SiC junctions to isolate the remaining PbS-QD/SiC interface. This enabled separate examination using localized illumination for scanning photocurrent microscopy (SPCM).[14,15] The architecture presented in Figure 1 enabled us to exploit the following phenomenological observations to achieve this: (i) ohmic contacts of graphene to ethanedithiol (EDT)-capped PbS QDs in air, consistent with p-type conduction reported previously,[21] which was also verified in the current work; (ii) a robust and ideal Schottky diode of EG/SiC[22] that is shown in this paper to be completely recoverable by selective chemical removal using hydrofluoric acid; (iii) a 10−15 monolayer (ML) EG film that achieves optical transparency for optoelectronic characterization,[14] while having a thickness greater than 1−2 ML screening length, such that electrostatic screening of the EG/SiC rectifying junction from the ohmic EG/PbS-QD film junction is achieved, precluding any potential barristor action.[19,20] This confluence of favorable conditions eliminates uncertainties stemming from the reproducibility of contacts between samples and between successive PbS-QD film depositions.

Our group has previously shown that gel permeation chromatography (GPC) is a precise and repeatable method for removing small molecule impurities from many types of QD samples.[23−25] Here, we employ GPC-purified PbS QDs to form spin-coated layers, in contrast to previous work on QD optoelectronic devices that has relied on precipitation and redissolution steps employing polar antisolvents.

EXPERIMENTAL SECTION

The device structure (Figure 1a) starts with EG/SiC Schottky diodes created by growing a homoepitaxial layer of n-type 4H-SiC, unintentionally doped to 1.6×10^{14} cm^{-3} on a n^+-SiC substrate by chemical vapor deposition (CVD) in a hot wall reactor with SiF_4 and propane precursors in a hydrogen atmosphere, as described elsewhere.[26−29] Graphene was then formed natively on the previous homoepitaxial layer through exposure to SiF_4 in an Ar atmosphere.[28] EG showed the key Raman peaks at ∼1580, ∼1350, and ∼2650 cm^{-1} with a D/G ratio of ∼0.1, indicating good quality. The thickness from X-ray photoelectron spectroscopy was ∼15 monolayers.[26,30] Individual circular device mesas with diameters ∼250 μm were fabricated by using standard photolithography and O_2-plasma reactive ion etching.

PbS QDs with a diameter of ∼4.5 nm and lowest energy exciton peak position at 1280 nm (∼0.97 eV) (Figure S1) were synthesized by following Zhang et al.[1] Following synthesis, the QDs, initially protected by alkyl carboxylate (oleate) surface coating, were purified by GPC.[23] A thin film was formed on the bare Schottky device by spin-coating, followed by in situ ligand exchange with ethanedithiol

DOI: 10.1021/acsaelm.9b00651
ACS Appl. Electron. Mater. 2020, 2, 134−139

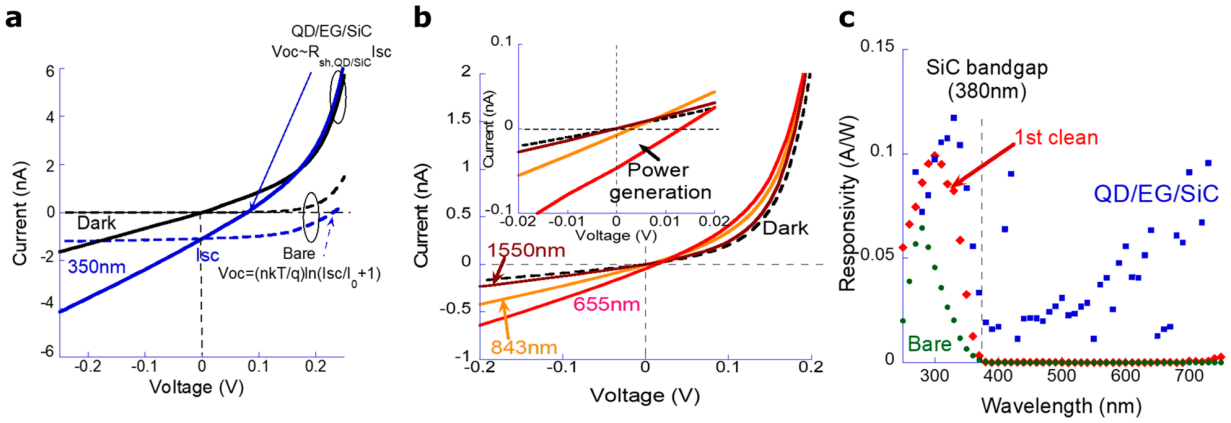

Figure 2. (a) Dark and 350 nm (UV) illuminated $I-V$ curves for the bare EG/SiC and hybrid QD film devices. (b) Dark and illuminated $I-V$ curves for the hybrid QD film device under 1550, 843, and 655 nm illumination at ~0.36 mW/cm^2. Inset: magnified view of power-generating quadrant. (c) Responsivity vs wavelength at low frequency under wide-area illumination for EG/SiC Schottky diode before application of the QD film, after QD film deposition, and after removal of QD film via chemical etching. All data were collected at $V = -1$ V.

(Figure S1)[31] in a N_2-filled glovebox. Following QD film deposition, contact was made to EG by locally puncturing the film with a tungsten probe tip and contact to the n^+-SiC substrate as made by using carbon tape.

The resulting film had a thickness of 90 nm, determined from atomic force microscopy (AFM) (Figure S1). Fourier-transform infrared spectroscopy was employed to confirm removal of the initial oleate ligand coating as has been reported previously for EDT solid-state exchange.[10,31,32] We found the QD film could be removed using 51% aqueous hydrofluoric acid and a new QD-film respun with qualitatively reproducible results (Figure 2c) where the device responsivity at photon energies below the SiC bandgap is dependent on the presence of the QD film.

RESULTS AND DISCUSSION

The EG/SiC Schottky diodes prior to QD deposition were evaluated by dc current−voltage ($I-V$) measurements (Figure 1b), and they displayed rectification in accordance with thermionic emission:

$$I = AA^*T^2 \exp\left(-\frac{\Phi_b}{k_BT}\right)\left[\exp\left(\frac{qV_a}{nk_BT}\right) - 1\right] = I_0\left[\exp\left(\frac{qV_a}{nk_BT}\right) - 1\right] \quad (1)$$

giving a Schottky barrier height of $\Phi_b \sim 0.9$ eV and an ideality of $n \sim 1.1$.[33] Upon the addition of the QD film, the hybrid diodes demonstrated higher reverse leakage, ~10^2 more than without QDs, suggesting the presence of trap states.[34] The current under forward bias indicated the presence of a second, parallel barrier interface leading to additional forward current at <0.2 V. We associate this with carrier transport through the QD film at the diode periphery. Upon removal of the QD layer with HF, this feature disappeared and the reverse leakage reverted to the bare state, indicating the changes were due to the QD film. We note that ultraviolet photoelectron spectroscopy measurements have revealed an electron affinity of 3.6 eV for 4H-SiC and a work function of ~4.5 eV for EDT-exchanged PbS QDs in previous reports.[9,35,36] Consistent with these findings, we propose band alignments as shown in Figure 1c.

To obtain the effective $I-V$ curve of the parallel current, the bare EG/SiC current was subtracted from the total current in the hybrid case (Figure 1c), isolating the behavior of an additional QD/SiC diode at the edge of the device (Figure 1a). This parallel diode had a series resistance, $R_{s,QD}$, of 2.4 MΩ, a shunt resistance, $R_{sh,QD/SiC}$, of 200 MΩ attributed to trapping at the interface and a diode element with a reverse saturation current, $I_{0,QD/SiC}$, of 4 pA, and an ideality $n = 2$, obtained by subtracting the $R_{s,QD}$ voltage drop. This indicates that the QD/SiC diode exhibits Shockley−Read−Hall (SRH) trap-assisted recombination,[37] in contrast to the $n \approx 1$ ideal behavior from the EG/SiC diode. At diode voltage $V_a < 0.2$ V, $R_{sh,QD/SiC}$ dominates the current and is likely due to a field-activated trapping mechanism at the QD/SiC interface. Trapping effects are further supported by the emergence of Lorentzian $1/f^2$ noise compared to $1/f$ flicker noise for the bare diode (Figure S2). The $1/f^2$ Lorentzian noise is an indicator of well-defined trap levels causing noise from variations in carrier concentration due to trapping/detrapping.[34,38−40]

The bare EG/SiC diodes displayed a photovoltaic response at photon energies above the 4H-SiC bandgap (3.2 eV) (Figure 2a), giving an open circuit voltage (V_{OC}) of ~0.25 V with 13 nW of 350 nm illumination. This agrees with the I_0 measured from the forward $I-V$ curves:

$$V_{OC} = \frac{nk_BT}{q}\ln\left(\frac{I_{SC}}{I_0} + 1\right) \quad (2)$$

With the addition of the QD film, V_{OC} and I_{SC} both decrease under the same UV illumination conditions. This is expected due to filtering of the incident light by the QD layer. Additionally, the QD layer introduces parallel conduction via $R_{sh,QD/SiC}$, with V_{OC} approximated by $V_{OC} \approx I_{SC}R_{sh,QD/SiC}$ in the limit of low I_{SC}.

Upon illumination with visible light below the SiC bandgap, parallel conduction via $R_{sh,QD/SIC}$ similar to the UV case is seen, but a photovoltaic effect is retained, attributed to the low-barrier rectifying QD/SiC junction after QD deposition. To confirm that the photocurrent was associated with light absorption in the QD layer, three LEDs were used with λ_{max} = 655, 843, and 1550 nm, adjusted so ~180 nW fell within the EG mesa. The measured I_{SC} (Figure 2b) were 50, 15, and <1 pA, respectively, with the trend in photocurrent matching the absorption spectrum of the QD film, which shows an effective

DOI: 10.1021/acsaelm.9b00651
ACS Appl. Electron. Mater. 2020, 2, 134−139

bandgap of ∼1350 nm corresponding to the lowest-energy electronic transition of the QDs (Figure S1a).

The QD film also exhibits significant photoconductivity with reverse bias. Both the dark current (I_{dark}) and photocurrent ($I_{ph} = I(\lambda) - I_{dark}$) of the hybrid device increase monotonically with voltage, indicating the presence of carrier traps and leading to the observed photoconductive gain.[34] This increase in I_{ph} was accompanied by an increase in the lifetime measured by transient photocurrent decay under wide-area illumination at 444 nm (Figure S3). For short circuit conditions, a lifetime of ∼40 ms described the decay well (Figure S3). As the reverse bias was increased, an additional slower lifetime emerged, increasing to 4.1 s at −1.0 V, but the faster component continued to dominate the photocurrent decay amplitude, increasing to 130 ms over the same bias range.

Figure 3 shows SPCM maps of a representative hybrid device, measured with 444 nm light chopped at 113 Hz.

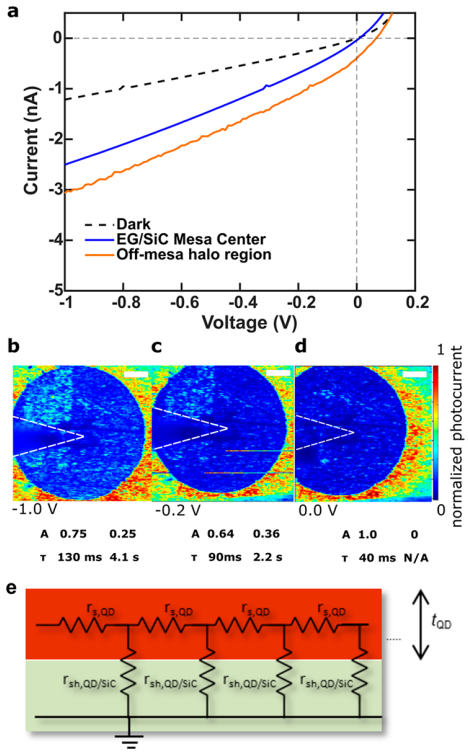

Figure 3. (a) Current−voltage response under localized 444 nm excitation (∼15 μW) for hybrid device; SPCM maps recorded at −1.0 V (b), −0.2 V (c), and 0 V for a short circuit (d) illustrating the spatial dependence of ac photocurrent from chopped light. Color scale is normalized to peak ac value at the edge of the mesa. The dashed line indicates the location of tungsten probe contact. White scale bars: 50 μm. Characteristic lifetimes and relative amplitudes for photocurrent decay accompany each image. (e) Transmission line model for series and shunt resistance contributions of the QD film.

Without the QD layer, the SPCM signal was confined to the EG mesa (Figure S4). After QD deposition, there was a sharp increase in I_{ph} near the periphery that was much greater than within the EG/SiC mesa. Outside the mesa, I_{ph} decays slowly with distance, retaining half its value at ∼80 μm at short circuit. The decay in I_{ph} with distance was accompanied by only a small change in phase (Figure S5), suggesting the decay is not of capacitive origin.

The diminished signal from on-mesa excitation indicates that the QD/EG junction is not responsible for the I_{ph} and I_{SC} under wide-area illumination: instead, the junction between the QD film and the n-type 4H-SiC epilayer is the active region. This effect is particularly notable at short circuit and under ac excitation as employed in SPCM, where photoconductive behavior is less significant. The considerable distance over which charge can be collected and the insensitivity of the decay length to applied bias (Figure 3b−d and Figure S6) suggest that the decay is not the minority carrier diffusion length but instead reflect an increasing series resistance for excitation further away from the EG contact. In this case, a transmission line model (TLM, Figure 3e)[41] can be applied to describe the equivalent circuit in Figure 1. Here, we assume that currents are low enough that $R_{sh,QD/SiC}$ and $R_{s,QD}$ dominate the behavior, meaning the diodes have not turned on. Under these conditions the TLM predicts an exponential decay of photocurrent with distance from the EG mesa contact, with characteristic (1/e) length L_T:[42]

$$L_T = \sqrt{\rho_{sh,QD/SiC}(t_{QD}/\rho_{s,QD})} \quad (3)$$

where t_{QD} is the thickness of the QD film, $\rho_{s,QD}$ is the (3D) resistivity of the QD film, and $\rho_{sh,QD/SiC}$ is a specific interface resistance at the QD/SiC interface, defined such that $R_{sh,QD/SiC} = \rho_{sh,QD/SiC}/A_{QD/SiC}$, with $A_{QD/SiC}$ the effective interface area. The SPCM maps in Figure 3 give $L_T \sim 115$ μm near $V_a = 0$ V. To approximate the effective interface area, we consider a ring of width L_T surrounding the mesa of radius r so that $A_{QD/SiC} = 2\pi r L_T + \pi L_T^2$. Using $R_{sh,QD/SiC} \sim 200$ MΩ (Figure 1), $\rho_{sh,QD/SiC} \sim 260$ kΩ·cm^2, $t_{QD} \sim 90$ nm (Figure S1), and solving eq 3 for $\rho_{s,QD}$ gives $\rho_{s,QD} \approx 18$ kΩ·cm, which is consistent with lateral $I-V$ measurements of the resistance between two neighboring EG mesas, conducting through the QD film (Figure S8).

In measurements of PbS QD films prepared using the same procedure on insulating substrates, we found ohmic contacts to evaporated top electrodes composed of high-workfunction metals, notably Au (Figure S8). Taken together, these observations identify the PbS QD film as a p-type semiconductor. Considering that field-effect hole mobilities $\mu \sim 10^{-3}$ cm^2/(V s) have been reported for EDT-capped PbS QD films,[11] the bulk resistivity identified from L_T corresponds to a hole concentration $\sim 10^{17}-10^{18}$ cm^{-3} in the present case.

Based on the above insights, there are design considerations that emerge for making practical solar cells and detectors from hybrid QD/EG/SiC devices: First, the highest I_{ph} comes from the QD/SiC junction, and designs should aim to maximize the incident light on this junction while maintaining charge collection via contacts. In this study, the EG forms an effective ohmic contact to EDT-terminated PbS, while forming a Schottky junction to the SiC substrate with a very high shunt resistance. The observation of minimal charge separation at the PbS QD-EG junction is consistent with some previous work on PbS QD-EG that found photoinduced charge transfer to be localized to the first few QD layers,[18] but we also observe lateral charge transport within the QD film over large distances. This indicates that EG electrodes in an interdigitated or grid structure separated by $\sim L_T$ could maximize both light absorption and charge collection. Third, the QD film thickness affects light absorption and charge transport but has not been optimized in the present devices. Films thinner than the diffusion length of carriers will collect the majority of photogenerated carriers, but if too thin, surface recombina-

DOI: 10.1021/acsaelm.9b00651
ACS Appl. Electron. Mater. 2020, 2, 134−139

tion[43,44] effects may suppress charge collection, particularly given the observed recombination in the presence of the QD film. The measured absorbance of ∼0.1 AU at λ = 655 nm for the 90 nm thick film indicates an absorption length $\alpha^{-1} \approx 390$ nm. Assuming L_T^2 scales linearly with t_{QD} as described by the TLM model in eq 3, a larger t_{QD} could enable a larger pitch between contacts. Finally, the measured lifetime ∼40 ms at short circuit would yield an electron diffusion length of ∼10 μm for a typical carrier mobility (μ) of $\sim 10^{-3}$ cm^2/(V s) in PbS-EDT. Independent measurement of carrier mobilities and diffusion lengths in QD films as a function of surface passivation and film deposition methods is an important target for future study.

CONCLUSIONS

We have shown that by integrating cheaply synthesized and tunable PbS QDs with a wide bandgap support, visible and IR functionality can be achieved in contexts previously not envisioned. By using QD films with EG/SiC Schottky diodes, we demonstrate photovoltaic action from IR to UV, both above and below the bandgap of SiC. The below-bandgap photovoltaic action is due to the formation of a parallel QD/SiC diode at the edge of the EG mesa, displaying above bandgap photovoltaic action. Because of the unoptimized nature of the QD/SiC interface, the specific interface resistance limits the open circuit voltage, attributed to trapping at the interface. Improvements can be made by increasing charge separation at the QD/SiC interface through optimized band alignment and surface treatment, reducing the resistivity of the QD film and increasing its thickness while maintaining a sufficiently large diffusion length. Importantly, new strategies are emerging for deposition of wide-bandgap materials of high quality including SiC[45] as well as patterning of EG films of sufficient quality to display quantum transport behavior.[18,46] With these insights, useful photovoltaic devices and photodetectors may be realized for QD/EG/SiC hybrid architectures, particularly in the IR, where wide-bandgap materials' advantages cannot often be exploited.

ASSOCIATED CONTENT

Supporting Information

The Supporting Information is available free of charge at https://pubs.acs.org/doi/10.1021/acsaelm.9b00651.

Additional materials and methods; Figures S1−S7 (PDF)

AUTHOR INFORMATION

Corresponding Authors

*E-mail greytak@sc.edu.
*E-mail chandra@cec.sc.edu.

ORCID

Andrew B. Greytak: 0000-0001-8978-6457

Present Address

C.A.L.-B.: Department of Mechanical and Aerospace Engineering, University of Virginia.

Author Contributions

M.L.K. and J.L. contributed equally to this work.

Notes

The authors declare no competing financial interest.

ACKNOWLEDGMENTS

This research work is partially supported by National Science Foundation (NSF), ECCS Award Nos. 1711322 and 1810116 under the supervision of program director Dr. Dimitri Pavlidis. M.L.K. and J.L. were additionally supported by NSF IGERT graduate fellowships under Grant No. 1250052. The authors acknowledge partial support of this work by ARO Contract W911NF-18-1-0029 monitored by Dr. M. Gerhold. The authors also acknowledge the support from the University of South Carolina through the ASPIRE program. We thank Adam Roberge for helpful discussions on PbS QD purification, Anusha Balachandran for material growth, Surya Chava for device fabrication, and Richard Floyd for help with data processing.

REFERENCES

(1) Zhang, J.; Crisp, R. W.; Gao, J.; Kroupa, D. M.; Beard, M. C.; Luther, J. M. Synthetic Conditions for High-Accuracy Size Control of PbS Quantum Dots. *J. Phys. Chem. Lett.* **2015**, *6* (10), 1830−1833.

(2) Moreels, I.; Lambert, K.; Smeets, D.; De Muynck, D.; Nollet, T.; Martins, J. C.; Vanhaecke, F.; Vantomme, A.; Delerue, C.; Allan, G.; Hens, Z. Size-Dependent Optical Properties of Colloidal PbS Quantum Dots. *ACS Nano* **2009**, *3* (10), 3023−3030.

(3) Tvrdy, K.; Kamat, P. V. Quantum Dot Solar Cells. In *Comprehensive Nanoscience and Technology*; Academic Press: 2010; Vols. *1*−*5*, pp 257−275.

(4) Kamat, P. V. Quantum Dot Solar Cells. Semiconductor Nanocrystals as Light Harvesters. *J. Phys. Chem. C* **2008**, *112* (48), 18737−18753.

(5) King, L. A.; Riley, D. J. Importance of QD Purification Procedure on Surface Adsorbance of QDs and Performance of QD Sensitized Photoanodes. *J. Phys. Chem. C* **2012**, *116* (5), 3349−3355.

(6) Turyanska, L.; Makarovsky, O.; Svatek, S. A.; Beton, P. H.; Mellor, C. J.; Patanè, A.; Eaves, L.; Thomas, N. R.; Fay, M. W.; Marsden, A. J.; Wilson, N. R. Ligand-Induced Control of Photoconductive Gain and Doping in a Hybrid Graphene−Quantum Dot Transistor. *Adv. Electron. Mater.* **2015**, *1* (7), 1500062.

(7) Campbell, S. A. The Science and Engineering of Microelectronic Fabrication (The Oxford Series in Electrical and Computer Engineering), 2001.

(8) Brown, P. R.; Kim, D.; Lunt, R. R.; Zhao, N.; Bawendi, M. G.; Grossman, J. C.; Bulović, V. Energy Level Modification in Lead Sulfide Quantum Dot Thin Films through Ligand Exchange. *ACS Nano* **2014**, *8* (6), 5863−5872.

(9) Kroupa, D.; Beard, M.; et al. Tuning Colloidal Quantum Dot Band Edge Positions through Solution-Phase Surface Chemistry Modification. *Nat. Commun.* **2017**, *8*, 1−8.

(10) Konstantatos, G.; Badioli, M.; Gaudreau, L.; Osmond, J.; Bernechea, M.; De Arquer, F. P. G.; Gatti, F.; Koppens, F. H. L. Hybrid Graphene−Quantum Dot Phototransistors with Ultrahigh Gain. *Nat. Nanotechnol.* **2012**, *7* (6), 363.

(11) Klem, E. J. D.; Shukla, H.; Hinds, S.; MacNeil, D. D.; Levina, L.; Sargent, E. H. Impact of Dithiol Treatment and Air Annealing on the Conductivity, Mobility, and Hole Density in PbS Colloidal Quantum Dot Solids. *Appl. Phys. Lett.* **2008**, *92* (21), 212105.

(12) Omar, S. U.; Sudarshan, T. S.; Rana, T. A.; Song, H.; Chandrashekhar, M. V. S. Interface Trap-Induced Nonideality in as-Deposited Ni/4H-SiC Schottky Barrier Diode. *IEEE Trans. Electron Devices* **2015**, *62* (2), 615−621.

(13) Chava, V. S. N.; Omar, S. U.; Brown, G.; Shetu, S. S.; Andrews, J.; Sudarshan, T. S.; Chandrashekhar, M. V. S. Evidence of Minority Carrier Injection Efficiency > 90% in an Epitaxial Graphene/SiC Schottky Emitter Bipolar Junction Phototransistor for Ultraviolet Detection. *Appl. Phys. Lett.* **2016**, *108* (4), 043502.

(14) Chava, V. S. N.; Barker, B. G.; Balachandran, A.; Khan, A.; Simin, G.; Greytak, A. B.; Chandrashekhar, M. V. S. High Detectivity

DOI: 10.1021/acsaelm.9b00651
ACS Appl. Electron. Mater. 2020, 2, 134−139

Visible-Blind SiF4grown Epitaxial Graphene/SiC Schottky Contact Bipolar Phototransistor. *Appl. Phys. Lett.* **2017**, *111* (24), 243504.
(15) Barker, B. G., Jr.; Chava, V. S. N.; Daniels, K. M.; Chandrashekhar, M. V. S.; Greytak, A. B. Sub-Bandgap Response of Graphene/SiC Schottky Emitter Bipolar Phototransistor Examined by Scanning Photocurrent Microscopy. *2D Mater.* **2018**, *5* (1), 011003.
(16) Sun, Z.; Liu, Z.; Li, J.; Tai, G.; Lau, S.; Yan, F. Infrared Photodetectors Based on CVD-grown Graphene and PbS Quantum Dots with Ultrahigh Responsivity. *Adv. Mater.* **2012**, *24* (43), 5878−5883.
(17) Robin, A.; Lhuillier, E.; Xu, X. Z.; Ithurria, S.; Aubin, H.; Ouerghi, A.; Dubertret, B. Engineering the Charge Transfer in All 2D Graphene-Nanoplatelets Heterostructure Photodetectors. *Sci. Rep.* **2016**, *6* (1), 24909.
(18) Makarovsky, O.; Turyanska, L.; Mori, N.; Greenaway, M.; Eaves, L.; Patané, A.; Fromhold, M.; Lara-Avila, S.; Kubatkin, S.; Yakimova, R. Enhancing Optoelectronic Properties of SiC-Grown Graphene by a Surface Layer of Colloidal Quantum Dots. *2D Mater.* **2017**, *4* (3), No. 031001.
(19) Yu, T.; Wang, F.; Xu, Y.; Ma, L.; Pi, X.; Yang, D. Graphene Coupled with Silicon Quantum Dots for High-Performance Bulk-Silicon-Based Schottky-Junction Photodetectors. *Adv. Mater.* **2016**, *28*, 4912−4919.
(20) Jahangir, I.; Uddin, M. A.; Singh, A. K.; Koley, G.; Chandrashekhar, M. V. S. S. Richardson Constant and Electrostatics in Transfer-Free CVD Grown Few-Layer MoS2/Graphene Barristor with Schottky Barrier Modulation> 0.6 EV. *Appl. Phys. Lett.* **2017**, *111* (14), 142101.
(21) Graetzel, M.; Janssen, R. A. J.; Mitzi, D. B.; Sargent, E. H. Materials Interface Engineering for Solution-Processed Photovoltaics. *Nature* **2012**, *488*, 304−312.
(22) Rana, T.; Chandrashekhar, M. V. S.; Daniels, K.; Sudarshan, T. Epitaxial Growth of Graphene on SiC by Si Selective Etching Using SiF4 in an Inert Ambient. *Jpn. J. Appl. Phys.* **2015**, *54* (3), 030304.
(23) Shen, Y.; Gee, M. Y.; Tan, R.; Pellechia, P. J.; Greytak, A. B. Purification of Quantum Dots by Gel Permeation Chromatography and the Eeffect of Excess Ligands on Shell Growth and Ligand Exchange. *Chem. Mater.* **2013**, *25* (14), 2838−2848.
(24) Shen, Y.; Roberge, A.; Tan, R.; Gee, M. Y.; Gary, D. C.; Huang, Y.; Blom, D. A.; Benicewicz, B. C.; Cossairt, B. M.; Greytak, A. B. Gel Permeation Chromatography as a Multifunctional Processor for Nanocrystal Purification and On-Column Ligand Exchange Chemistry. *Chem. Sci.* **2016**, *7* (9), 5671−5679.
(25) Roberge, A.; Stein, J. L.; Shen, Y.; Cossairt, B. M.; Greytak, A. B. Purification and In Situ Ligand Exchange of Metal-Carboxylate-Treated Fluorescent InP Quantum Dots via Gel Permeation Chromatography. *J. Phys. Chem. Lett.* **2017**, *8* (17), 4055−4060.
(26) Balachandran, A. High Quality Low Offcut 4H-SiC Epitaxy and Integrated Growth of Epitaxial Graphene for Hybrid Graphene/SiC Devices. PhD Thesis, University of South Carolina, Columbia, SC, 2017.
(27) Balachandran, A.; Song, H. Z.; Sudarshan, T. S.; Shetu, S. S.; Chandrashekhar, M. V. S. Study of SiC Epitaxial Growth Using Tetrafluorosilane and Dichlorosilane in Vertical Hotwall CVD Furnace. *Mater. Sci. Forum* **2015**, *821−823*, 137−140.
(28) Rana, T.; Chandrashekhar, M. V. S.; Daniels, K.; Sudarshan, T. SiC Homoepitaxy, Etching and Graphene Epitaxial Growth on SiC Substrates Using a Novel Fluorinated Si Precursor Gas (SiF 4). *J. Electron. Mater.* **2016**, *45* (4), 2019−2024.
(29) Shetu, S. S.; Omar, S. U.; Daniels, K. M.; Daas, B.; Andrews, J.; Ma, S.; Sudarshan, T. S.; Chandrashekhar, M. V. S. Si-Adatom Kinetics in Defect Mediated Growth of Multilayer Epitaxial Graphene Films on 6H-SiC. *J. Appl. Phys.* **2013**, *114* (16), 164903.
(30) Balachandran, A.; Song, H.; Sudarshan, T. S.; Chandrashekhar, M. V. S. 4H−SiC Homoepitaxy on Nearly on-Axis Substrates Using TFS-towards High Quality Epitaxial Growth. *J. Cryst. Growth* **2016**, *448*, 97−104.
(31) Klem, E. J. D.; MacNeil, D. D.; Cyr, P. W.; Levina, L.; Sargent, E. H. Efficient Solution-Processed Infrared Photovoltaic Cells: Planarized All-Inorganic Bulk Heterojunction Devices via Inter-Quantum-Dot Bridging during Growth from Solution. *Appl. Phys. Lett.* **2007**, *90* (18), 183113.
(32) Bessonov, A. A.; Allen, M.; Liu, Y.; Malik, S.; Bottomley, J.; Rushton, A.; Medina-Salazar, I.; Voutilainen, M.; Kallioinen, S.; Colli, A.; Bower, C.; Andrew, P.; Ryhänen, T. Compound Quantum Dot−Perovskite Optical Absorbers on Graphene Enhancing Short-Wave Infrared Photodetection. *ACS Nano* **2017**, *11* (6), 5547−5557.
(33) Zaman, M. Y.; Perrone, D.; Ferrero, S.; Scaltrito, L.; Naretto, M. Evaluation of Correct Value of Richardson's Constant by Analyzing the Electrical Behavior of Three Different Diodes at Different Temperatures. *Mater. Sci. Forum* **2012**, *711*, 174−178.
(34) Konstantatos, G.; Sargent, E. H. PbS Colloidal Quantum Dot Photoconductive Photodetectors: Transport, Traps, and Gain. *Appl. Phys. Lett.* **2007**, *91* (17), 173505.
(35) Brown, P. R.; Kim, D.; Lunt, R. R.; Zhao, N.; Bawendi, M. G.; Grossman, J. C.; Bulovi, V. Energy Level Modi Fi Cation in Lead Sul Fi de Quantum Dot Thin Films through Ligand Exchange. *ACS Nano* **2014**, *8* (6), 5863−5872.
(36) Wiets, M.; Weinelt, M.; Fauster, T. Electronic Structure of SiC (0001) Surfaces Studied by Two-Photon Photoemission. *Phys. Rev. B: Condens. Matter Mater. Phys.* **2003**, *68* (12), 125321.
(37) Sze, S. M.; Ng, K. K. *Physics of Semiconductor Devices*; John Wiley & Sons: 2006.
(38) Hooge, F. N. 1/f Noise Sources. *IEEE Trans. Electron Devices* **1994**, *41* (11), 1926−1935.
(39) Balandin, A. A. Low-Frequency 1/f Noise in Graphene Devices. *Nat. Nanotechnol.* **2013**, *8* (8), 549−555.
(40) Anghel, L.; Ouisse, T.; Billon, T.; Lassagne, P.; Jaussaud, C. Low Frequency Noise in Silicon Carbide Schottky Diodes. *Diamond Relat. Mater.* **1997**, *6* (10), 1494−1496.
(41) Al-Zeben, M. Y.; Saleh, A. H. M.; Al-Omar, M. A. TLM Modelling of Diffusion, Drift and Recombination of Charge Carriers in Semiconductors. *Int. J. Numer. Model. Electron. Netw. Devices Fields* **1992**, *5* (4), 219−225.
(42) Shatalov, M.; Simin, G.; Adivarahan, V.; Chitnis, A.; Wu, S.; Pachipulusu, R.; Mandavilli, V.; Simin, K.; Zhang, J. P.; Yang, J. W.; Khan, M. A. Lateral Current Crowding in Deep UV Light Emitting Diodes over Sapphire Substrates. *Jpn. J. Appl. Phys.* **2002**, *41* (8R), 5083.
(43) Henry, C. H. Limiting Efficiencies of Ideal Single and Multiple Energy Gap Terrestrial Solar Cells. *J. Appl. Phys.* **1980**, *51* (8), 4494−4500.
(44) Green, M. A. Limiting Efficiency of Bulk and Thin-film Silicon Solar Cells in the Presence of Surface Recombination. *Prog. Photovoltaics* **1999**, *7* (4), 327−330.
(45) Aldalbahi, A.; Li, E.; Rivera, M.; Velazquez, R.; Altalhi, T.; Peng, X.; Feng, P. X. A New Approach for Fabrications of SiC Based Photodetectors. *Sci. Rep.* **2016**, *6* (1), 1−10.
(46) El Fatimy, A.; Nath, A.; Kong, B. D.; Boyd, A. K.; Myers-Ward, R. L.; Daniels, K. M.; Jadidi, M. M.; Murphy, T. E.; Gaskill, D. K.; Barbara, P. Ultra-Broadband Photodetectors Based on Epitaxial Graphene Quantum Dots. *Nanophotonics* **2018**, *7* (4), 735−740.

DOI: 10.1021/acsaelm.9b00651
ACS Appl. Electron. Mater. 2020, 2, 134−139